Nonlinear Hybrid Simulation of Internal Kink with Beam Ion Effects in DIII-D

Wei Shen[1], G. Y. Fu[2], Benjamin Tobias[2], Michael Van Zeeland[3],

Feng Wang[4], and Zheng-Mao Sheng[1]

February 10, 2015

[1]Department of Physics, Institute for Fusion Theory and Simulation, Zhejiang University, Hangzhou 310027, China

[2]Princeton Plasma Physics Laboratory, Princeton, NJ 08543, USA

[3]General Atomics, San Diego, California 92186-5608, USA

[4]School of Physics and Optoelectronic Engineering, Dalian University of Technology, Dalian 116024, China

Abstract

In DIII-D sawteething plasmas, long-lived (1,1) kink modes are often observed between sawtooth crashes. The saturated kink modes have two distinct frequencies. The mode with higher frequency transits to a fishbone-like mode with sufficient on-axis neutral beam power. In this work, hybrid simulations with the global kinetic-magnetohydrodynamic (MHD) hybrid code M3D-K have been carried out to investigate the linear stability and nonlinear dynamics of the $n = 1$ mode with effects of energetic beam ions for a typical DIII-D discharge where both saturated kink mode and fishbone were observed. Linear simulation results show that the $n = 1$ internal kink mode is unstable in MHD limit. However, with kinetic effects of beam ions, a fishbone-like mode is excited with mode frequency about a few kHz depending on beam pressure profile. The mode frequency is higher at higher beam power and/or narrower radial profile consistent with the experimental observation. Nonlinear simulations have been performed to investigate mode saturation as well as energetic particle transport. The nonlinear MHD simulations show that the unstable kink mode becomes a saturated kink mode after a sawtooth crash. With beam ion effects, the fishbone-like mode can also transit to a saturated kink mode with a small but finite mode frequency. These results are consistent with the experimental observation of saturated kink mode between sawtooth crashes.

1 INTRODUCTION

There is much interest recently in the phenomena of internal three-dimensional (3D) deformations in magnetically confined fusion devices such as tokamak, reversed field pinch (REP) and spherical tokamak (ST). The examples of the 3D structures are termed as snakes, saturated kinks, long-lived modes (LLMs) and single helical axis (SHAx) configurations. The snakes, characterized by a localized region of plasma density that rotates within the field of view of various diagnostics, were first observed at the Joint European Torus (JET)[1, 2]. The standard model proposed by Wesson[3] suggests that the localized cooling of the $q = 1$ surface leads to the formation of a magnetic island, which traps the excess ions from the pellet and causes the formation of the snakes. Moreover, in Tore Supra the snake patterns were found to be radially located well inside the $q = 1$ surface[4], and the impurity-induced snakes observed on Alcator C-Mod suggest the importance to separate the dynamics between the plasma density and temperature[5]. In addition to snakes, a continuous dominantly $m = 1, n = 1$ mode emerges and persists after sawteeth oscillations in TCV[6, 7], and LLMs were observed in the Mega-Ampere Spherical Tokamak (MAST) with weakly reversed safety factor profile and minimum safety factor q_{min} just above unity[8]. The non-resonant internal kink mode (NRK) was also observed in the National Spherical Torus Experiment (NSTX)[9], and numerical simulations carried out by Breslau et al.[10] showed that the nonlinearly saturated $n = 1$ NRK in NSTX could induce a (2,1) magnetic island at the $q = 2$ surface[11]. Wang et al. then further investigated the linear and nonlinear dynamics of the NRK in NSTX considering toroidal rotation[12] and energetic particle effects[13]. Also in the RFX-mode reversed field pinch the SHAx state was reported[14]. The snakes, LLMs, SHAx, etc, as suggested by Cooper et al.[15, 16, 17], represent the same physical phenomenon: saturated dominantly $m = 1, n = 1$ internal kink modes.

The saturated kink mode is often closely associated with sawtooth oscillations.The mode can induce large fast ion transport and significant modification in the q profile[8, 18, 19]. As a result, understanding them is important for the operation of the International Thermonuclear Experimental Reactor (ITER) where the $q = 1$ radius could be as large as half of the minor radius.

Nonlinear saturated $m = 1, n = 1$ internal kinks have been investigated both analytically[20, 21, 22] and numerically[23, 24, 25]. Recently, Cooper et al. considered the saturated kinks as bifurcated equilibrium states[15, 16, 17] and analysed the 3D deformations by applying the equilibrium codes VMEC[26] and ANIMEC[27]. In this work, the global kinetic-magnetohydrodynamic (MHD) hybrid code M3D-K[28, 29] has been applied to investigate the dynamics of the $n = 1$ kink mode in DIII-D sawteething plasmas. Compared to previous work using single fluid model, this work includes the important kinetic effects of energetic beam ions using a kinetic-MHD hybrid model with realistic tokamak geometry and plasma profiles of a DIII-D discharge. Our results show that the existence of the saturated kink mode after an initial sawtooth crash. With beam ion kinetic effects, a fishbone-like mode is excited with mode frequency around a few kHz, and the mode frequency is larger with higher beam power and/or narrower radial profile of the beam pressure. These results are consistent with the experimental observation in the

DIII-D plasmas.

This article is organized as follows: Sec. II briefly introduces the M3D-K code and parameters used in this work. In Sec. III the MHD results of the $n = 1$ kink mode are presented. Sec. IV describes the simulation results of the fishbone-like mode with beam ion effects. Finally discussion and summary are given in Sec. V.

2   M3D-K MODEL AND BASIC PARAMETERS

This work is performed using the global kinetic-MHD hybrid code M3D-K[28, 29], in which the background thermal plasma is described by the resistive MHD model while the energetic particles are treated using drift kinetic equation. Particle-in-cell method[29] is employed for solving the drift kinetic equation. The M3D-K code has been extensively applied to study MHD modes and energetic particle instabilities in tokamaks[29, 30, 31, 32, 33, 12, 13, 34].

We consider a beam-heated discharge in DIII-D plasmas. As shown in Fig. 1, a spectrogram from localized ECE measurement near the $q = 1$ surface contains multiple $m = 1, n = 1$ oscillations between successive sawtooth crash events (solid vertical lines), including fishbone-like modes that chirp down in frequency from approximately 15.5 kHz to 14 kHz (A). An off-axis neutral beam source is added to on-axis neutral beam injection at $t = 3000\ ms$, elevating the toroidal carbon impurity rotation near the $q = 1$ surface. Equilibrium plasma profiles for these simulations are taken from $t = 3110\ ms$ (dashed vertical line). As the beam particle distribution becomes more broad with time, the fishbone relaxes to a constant frequency oscillation at around 14 kHz, growing in amplitude over time until the onset of sawtooth reconnection (B).
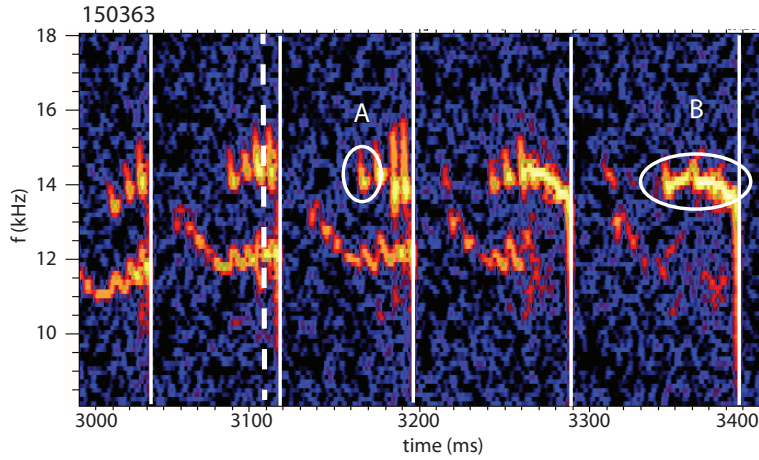

Figure 1: Spectrogram from localized ECE measurement near the $q = 1$ surface.

The main parameters and profiles in the DIII-D discharge are as follows: major radius $R_0 = 1.63\ m$, minor radius $a = 0.616\ m$, inverse aspect ratio $\epsilon \equiv a/R_0 = 0.378$, elongation $\kappa = 1.65$, triangularity $\delta = 0.036$, toroidal magnetic field $B_0 = 1.90\ T$, density $n_0 = 5.6 \times 10^{19}\ m^{-3}$, central thermal plasma beta $\beta_{thermal,0} = 3.40\%$, Alfvén

speed $v_A \equiv B_0/(\mu_0\rho_0)^{1/2} = 3.91 \times 10^6$ m/s, Alfvén time $\tau_A \equiv R_0/v_A = 4.17 \times 10^{-7}$ s. The resistivity profile is given by Spitzer form $\eta(T) = \eta_0(T/T_0)^{-3/2}$, where η_0 and T_0 are, respectively, the resistivity and temperature at the magnetic axis. The pressure profile is given by

$$P(\Psi) = P_{thermal,0}(1 - 2.432\Psi + 3.098\Psi^2 - 2.434\Psi^3 + 0.773\Psi^4) + P_{beam,0}\exp(-\Psi/\Delta\Psi), \qquad (1)$$

where $P_{thermal,0}$ and $P_{beam,0}$ are, respectively, the pressure of bulk plasma and energetic particles at the magnetic axis, and Ψ is the normalized poloidal flux variable varying from 0 at axis to 1 at the edge of the plasma. $P_{beam,0} = 0.49$ $P_{thermal,0}$, and $\Delta\Psi = 0.39$. The total pressure $P(\Psi)$ is used in the MHD simulation. The density profile is given by

$$n(\Psi) = n_0(1 - 0.5298\Psi - 1.348\Psi^2 + 3.361\Psi^3 - 2.1799\Psi^4), \qquad (2)$$

where n_0 is the density at the magnetic axis, and the density profile is assumed to be fixed with time. The safety factor profile is given by

$$q(\Psi) = 0.911 - 0.126\Psi + 4.299\Psi^2 - 7.678\Psi^3 + 7.127\Psi^4, \qquad (3)$$

with $q(0) = 0.911$ at the center and $q(1) = 4.533$ at the edge, and the $q = 1$ surface is located at $\Psi = 0.191$. Detailed profiles of safety factor, pressure and density are shown in Fig. 2.
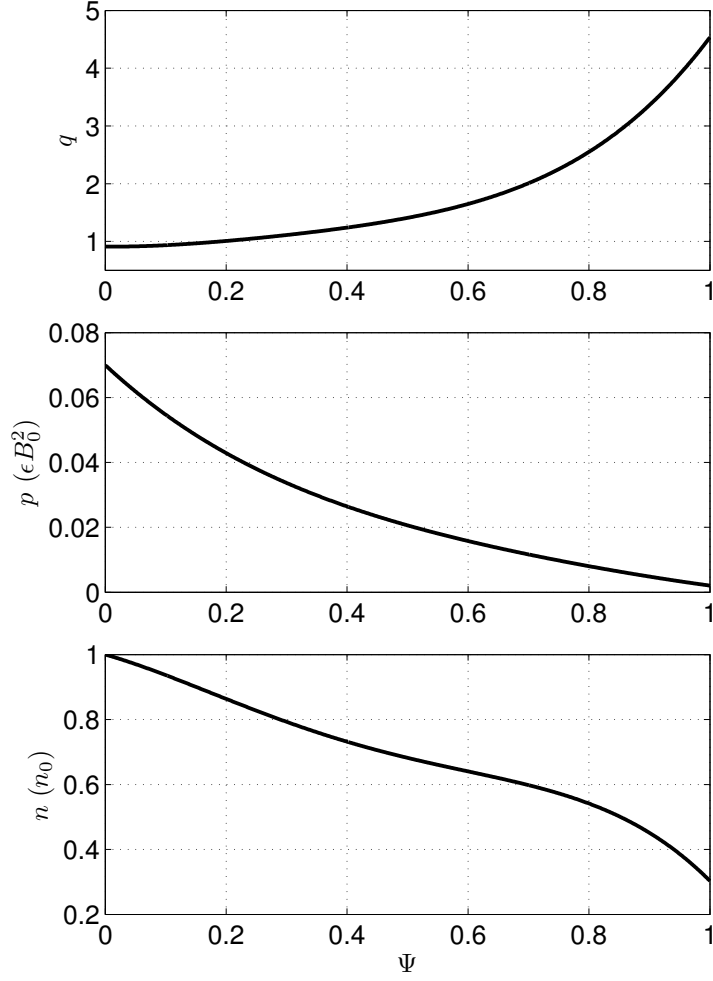
Figure 2: Equilibrium profiles of q, pressure and density.

The beam ions have a slowing-down distribution in energy, and are distributed exponentially in pitch angle and the radial direction,

$$f = \frac{cH(v_0 - v)}{v^3 + v_c^3} \exp(-(\Lambda - \Lambda_0)^2/\Delta\Lambda^2) \exp(-\langle\Psi\rangle/\Delta\Psi), \tag{4}$$

where c is a normalization factor, H is the step function, v_0 is the beam particle injection speed, v_c is the critical velocity given by

$$v_c^3 = \frac{3\sqrt{\pi}}{4} \frac{m_e}{m_i} (\frac{2T_e}{m_e})^{3/2}, \tag{5}$$

$\Lambda \equiv \mu B_0/E$ is the pitch angle parameter, $\Lambda_0 = 0.6$, $\Delta\Lambda = 0.3$, $\Delta\Psi = 0.39$, $\langle\Psi\rangle$ is Ψ averaged over the particle orbit. The beam ions consist of both co-passing and trapped particles, and the normalized particle speed and gyroradius are given by $v_0/v_A = 0.705$ and $\rho_h/a = 0.0429$.

3 MHD simulations

We consider here linear and nonlinear evolution of the n=1 mode in the MHD limit, i.e., the beam ions are described by MHD model and the kinetic effects of beam ions are neglected. The MHD results will be compared with the simulation results with beam ion kinetic effects in the next section.

First, linear MHD simulations of n=1 mode are performed for the given equilibrium. The results show an ideally unstable kink mode with linear growth rate $\gamma\tau_A = 0.0141$, this mode is mainly located inside the $q = 1$ rational surface with dominant mode number $n = m = 1$. Detailed mode structure is shown in Fig. 3 (a). The corresponding results with beam ion kinetic effects are shown in Fig. 3 (b) and (c) and will be discussed in next section.
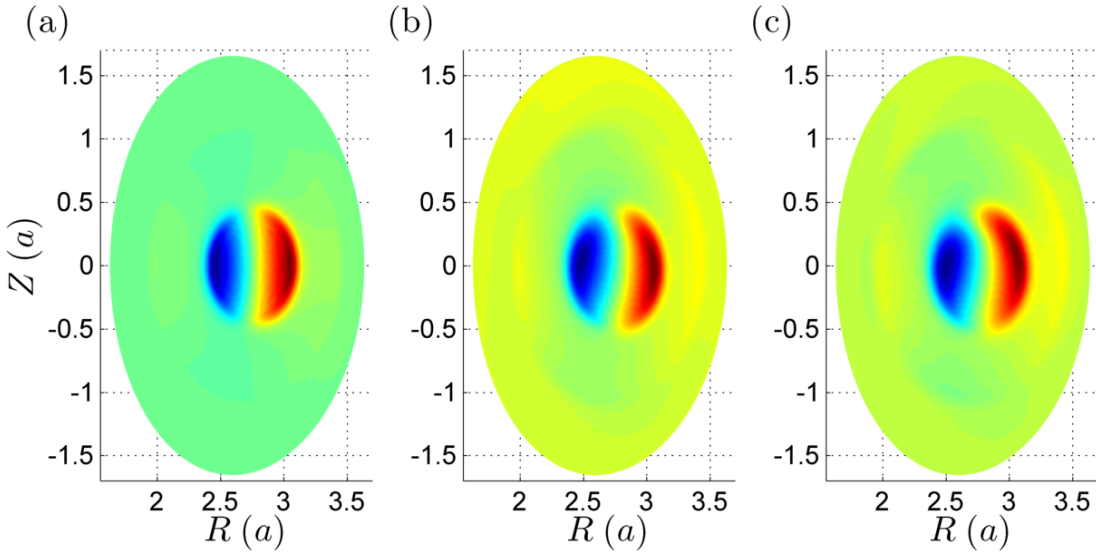

Figure 3: Velocity stream function U of the eigenmode. (a) Without energetic particles. (b) $\Delta\Psi = 0.39$ and $P_{beam,0}/P_{total,0} = 0.329$ with energetic particles. (c) $\Delta\Psi = 0.25$ and $P_{beam,0}/P_{total,0} = 0.418$ with energetic particles.

Now we turn to the nonlinear MHD simulation results. To initialize the simulation, the current and heat sources are prescribed to be consistent with the equilibrium current and pressure profiles. Here η_0 was set to be 10^{-5}, correspondingly the Lundquist number $S = 1/\eta_0 = 10^5$. The viscosity and perpendicular thermal conductivity were uniform and chosen to be, respectively, $\nu = 3 \times 10^{-5}$ ($\epsilon a V_A$) and $\chi_\perp = 3 \times 10^{-4}$ ($B_0^2 R_0/V_A$). We start the 3D nonlinear simulation with an $n = 1$ perturbation, which evolves into an $n = 1$ internal kink instability in the linear phase. As shown in Fig. 4, the time evolution of the central pressure P(0) and the kinetic energy of different toroidal modes indicates that the mode reaches a 3D quasi-steady state after the initial sawtooth crash, with the $n = 1$ mode being the dominant component. The corresponding Poincaré plots of magnetic surfaces during the saturated phase are almost stationary, and they are shown in Fig. 5 (a). The pressure profile at the same toroidal plane is shown in Fig. 6 (a), it is flatten inside the $q = 1$ surface and consistent with the structure of magnetic surfaces. In addition,

as shown in Fig. 7 (a), the corresponding q profile at the same time is flatten inside and almost equals unity. The results with beam ion kinetic effects (Fig. 5 (b), Fig. 5 (c), Fig. 6 (b), Fig. 6 (c)), Fig. 7 (b), and Fig. 7 (c) will be discussed in next section.
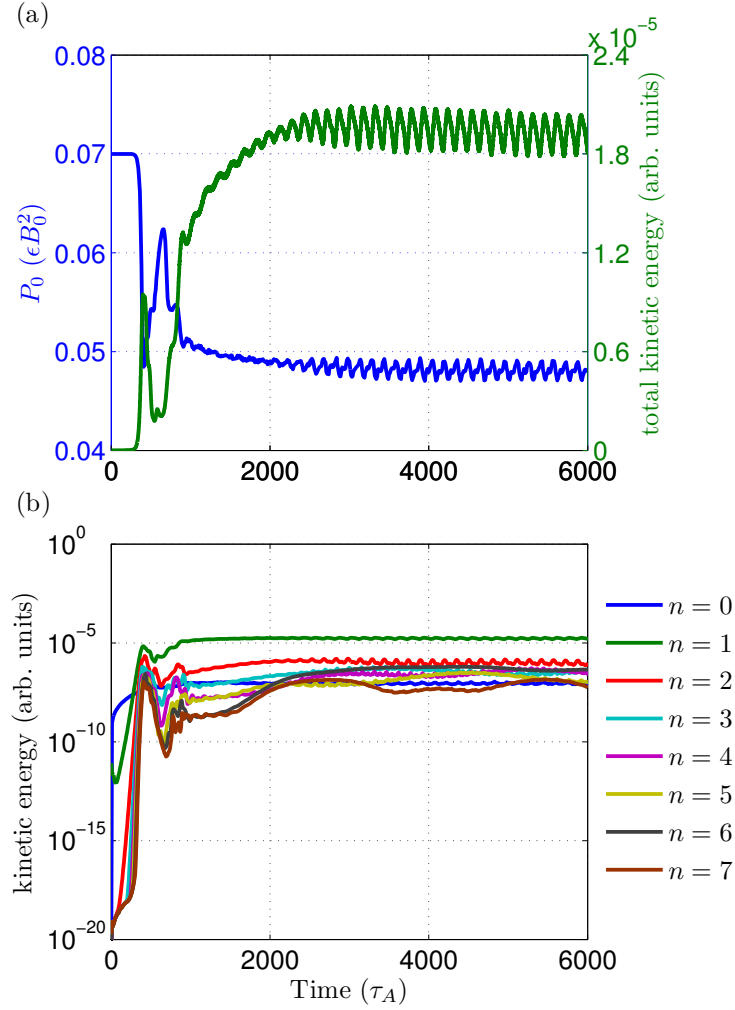

Figure 4: (a) Evolution of total kinetic energy and P(0). Time is normalized with the Alfvén time τ_A. (b) Kinetic energy evolution of different toroidal modes.
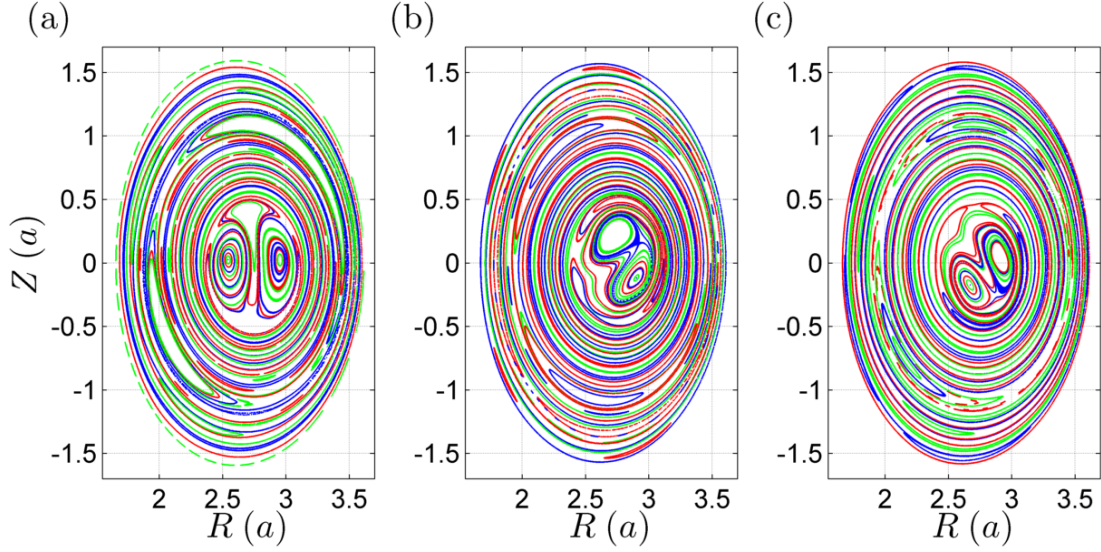
Figure 5: Poincaré plots of magnetic surfaces at the $\phi = \pi/2$ toroidal plane and at $t = 2300 \ \tau_A$. (a) Without energetic particles. (b) With energetic particles and $\Delta\Psi = 0.39$. (c) With energetic particles and $\Delta\Psi = 0.25$.
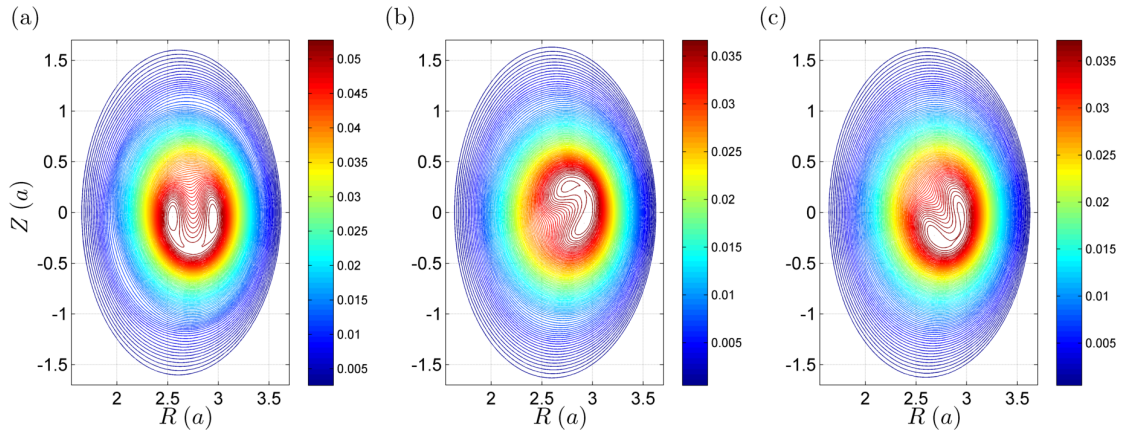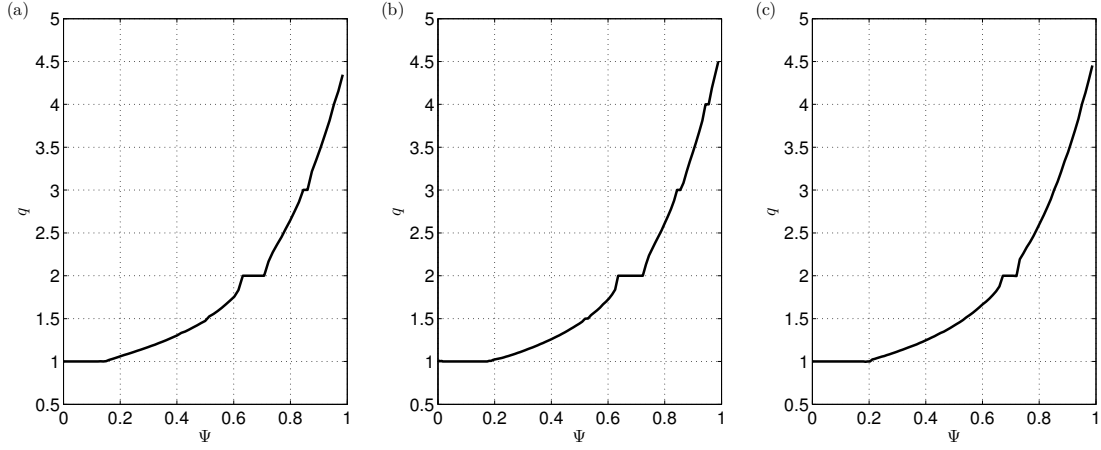

Figure 6: Pressure contour profiles at the $\phi = \pi/2$ toroidal plane and at $t = 2300 \ \tau_A$. (a) Without energetic particles. (b) With energetic particles and $\Delta\Psi = 0.39$. (c) With energetic particles and $\Delta\Psi = 0.25$.

Figure 7: q profiles at the $\phi = \pi/2$ toroidal plane and at $t = 2300 \ \tau_A$. (a) Without energetic particles. (b) With energetic particles and $\Delta\Psi = 0.39$. (c) With energetic particles and $\Delta\Psi = 0.25$.

Fig. 8 compares evolution of the $n = 1$ kinetic energy with and without high n components. It is shown that the $n = 1$ modes both saturate after the sawtooth crash, and high n components enhance the saturation level of the $n = 1$ kinetic energy.
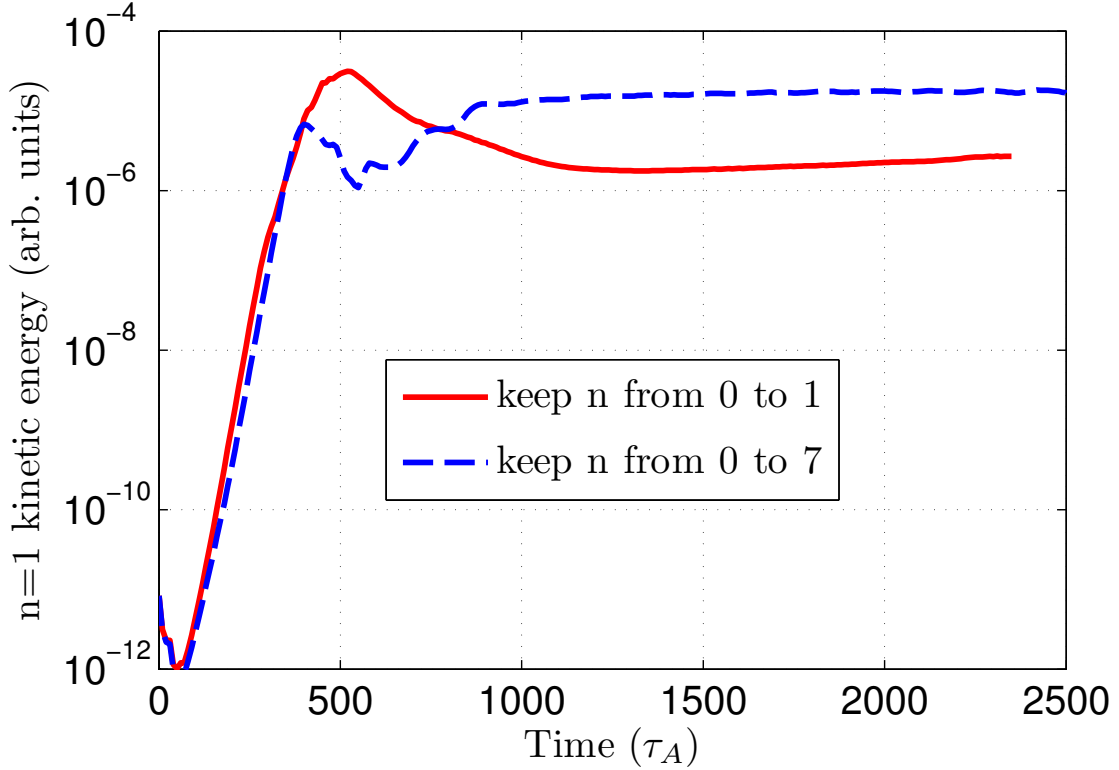
Figure 8: Evolution of the $n = 1$ kinetic energy. The solid line (red) shows simulation result with toroidal modes from $n = 0$ to $n = 1$, and the dashed line (blue) shows simulation result with toroidal modes from $n = 0$ to $n = 7$.

To investigate the dependence of the 3D quasi-steady state (or saturated kink) on the resistivity, we have performed the simulations with fixed ratio of the resistivity, viscosity and perpendicular thermal conductivity (i.e., $\nu/\eta_0 = 3$, and $\chi_\perp/\eta_0 = 30$). As shown in Fig. 9 (a), all cases reach 3D quasi-steady states for the resistivity range of $\eta_0 = 3.33 \times 10^{-6} \sim 9 \times 10^{-5}$. The corresponding kink saturation level varies from $U_{max} \sim 1.1 \times 10^{-3}$ $(\epsilon^2 v_A)$ to $U_{max} \sim 3.0 \times 10^{-3}$ $(\epsilon^2 v_A)$.

We now investigate the dependence of the existence of the saturated kink on the perpendicular thermal conductivity $\chi_\perp$. Fig. 9 (b) shows the nonlinear evolution of the kinetic energy for several values of $\chi_\perp$ at fixed resistivity and viscosity. We observe that when the perpendicular thermal conductivity decreases below a critical value, the quasi-steady state with the saturated kink mode transits from quasi-steady states of saturated kink to sawteeth cycles, similar to the previous results of Halpern et al.[25]. In their work, it was demonstrated that increasing the perpendicular thermal conductivity can trigger a transition from sustained sawtooth cycles to a 3D stationary equilibrium.
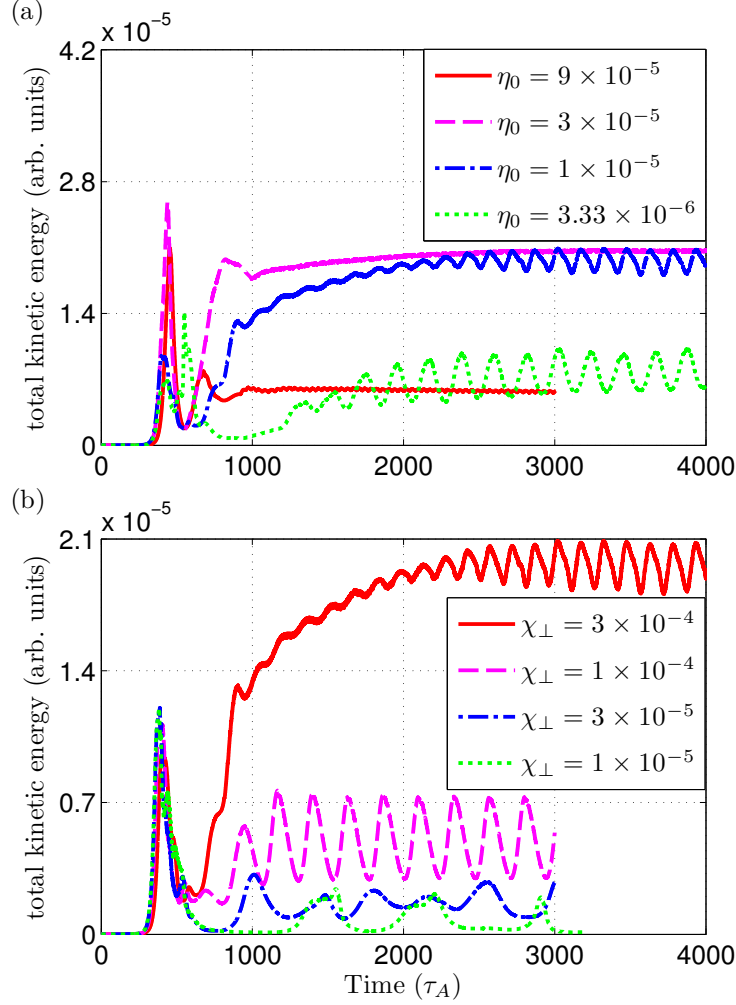
Figure 9: (a) Evolution of total kinetic energy with fixed ratio of the resistivity, viscosity and perpendicular thermal conductivity. (b) Evolution of total kinetic energy with different perpendicular thermal conductivity, keeping fixed resistivity and viscosity.

To summarize our MHD simulation results, we find that the nonlinear evolution of the n=1 kink mode results in a 3D quasi-steady state equilibrium of saturated kink for a DIII-D discharge. It should be noted that the ratio of $\chi_\perp/\eta_0 = 30$ used is realistic for the expected parameter of the experiment although the resistivity values used are much larger than the experimental value. The experimentally relevant resistivity values are computationally prohibitive for the code used and cannot be considered in this work.

4 Simulations with beam ion effects

We now consider in this section the kinetic effects of energetic beam ions on the $n = 1$ kink mode using the M3D-K code both linearly and nonlinearly. Both the linear and nonlinear simulation results are presented below.

4.1 Linear results

To study the dependence of linear stability on the beam power, Fig. 10 shows the mode frequency and linear growth rate of the $n = 1$ mode as a function of beam ion pressure fraction at the magnetic axis $P_{beam,0}/P_{total,0}$, with the thermal pressure $P_{thermal}$ kept fixed. When the beam pressure increases, both the mode frequency and linear growth rate become larger. As shown in Fig. 3 (a), the mode structure is up-down symmetric with zero mode frequency in the MHD limit. When the beam pressure is sufficient large, the mode transits from a MHD-like mode to fishbone-like mode with a finite mode frequency and twisted mode structure, as shown in Fig. 3 (b).
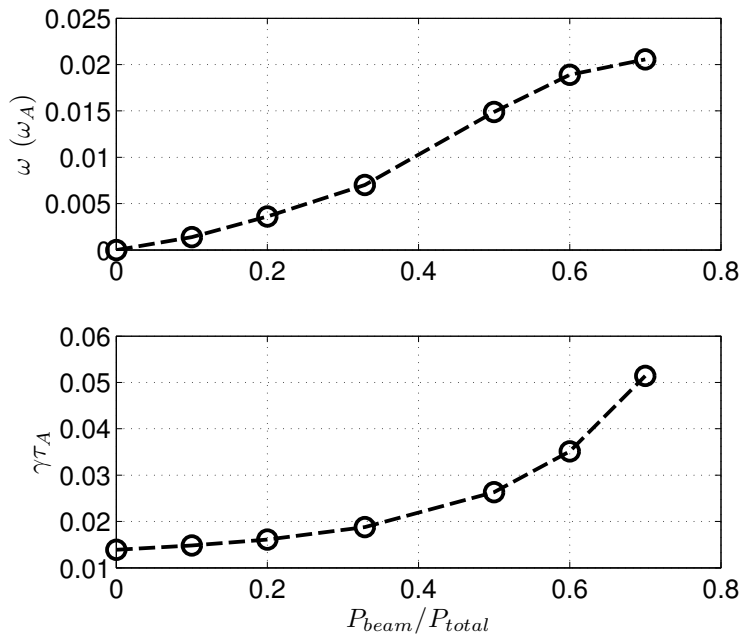

Figure 10: Mode frequency and linear growth rate as a function of $P_{beam,0}/P_{total,0}$ with $\Delta\Psi = 0.39$. $\omega_A \equiv 1/\tau_A$.

With the same $P_{thermal}$ and integrated beam pressure $\int_0^1 P_{beam} d\Psi$, the mode frequency and linear growth rate decreases when the radial profile of the beam pressure becomes broader, as shown in Fig. 11. Moreover, a narrower beam radial profile leads to a more twisted mode structure (Fig. 3 (c)) than that of a broader profile(Fig. 3 (b)).
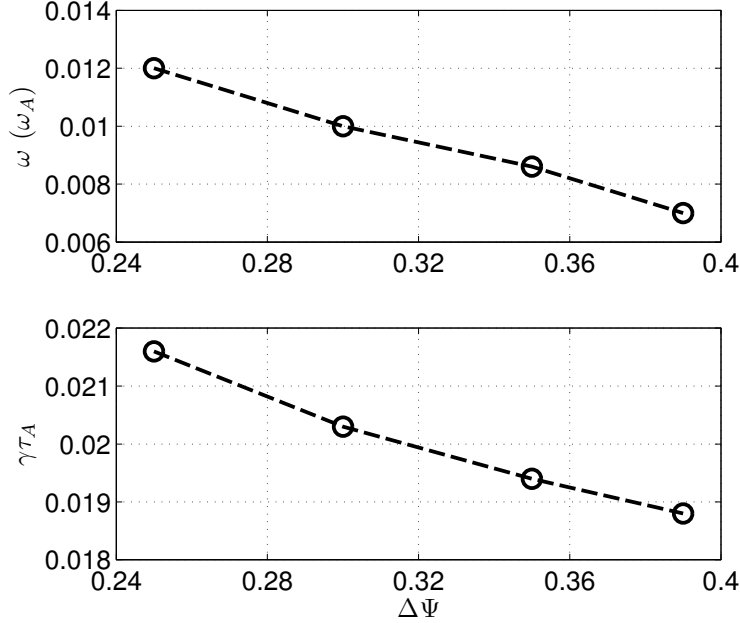
Figure 11: Mode frequency and linear growth rate versus different $\Delta\Psi$, with the same $P_{thermal}$ and $\int P_{beam}d\Psi$.

It should be pointed out the finite mode frequency is induced by the non-adiabatic response of beam ions. Furthermore the calculated mode frequencies in Fig. 10 and Fig. 11 correspond to frequencies of a few kHz in the plasma frame consistent with experimental measurement. Furthermore the simulated dependence of mode frequency on beam ion profile agree qualitatively with the measured trend of fishbone excitation. In the experiment, the fishbone tends to be excited with higher beam power and narrower beam radial profile (i.e., on-axis heating).

4.2   Nonlinear results

We now present nonlinear results with beam ion kinetic effects. Two radial profiles of the beam ion pressure with the same $P_{thermal}$ and $\int_0^1 P_{beam}d\Psi$ are chosen for the nonlinear simulation. As given by Eqs. (1) and (4), $\Delta\Psi = 0.39$ with $P_{beam,0}/P_{total,0} = 0.329$, and $\Delta\Psi = 0.25$ with $P_{beam,0}/P_{total,0} = 0.418$ are respectively used. Fig. 12 show that the mode also saturates as a 3D quasi-steady state after the initial sawtooth crash for both cases, with the $n = 1$ mode being the dominant one. Compared with the corresponding MHD nonlinear results, The Poincaré plots of magnetic surfaces during the saturated phase are similar. The only difference is that, with energetic beam ions, the structure of magnetic surfaces rotates with a finite frequency as shown in Figs. 5 (b) and Fig. 5 (c). Similarly, the corresponding pressure profiles at the same plane (shown in Figs. 6 (b) and Fig. 6 (c)) are flatten inside the $q = 1$ surface and consistent with the structure of magnetic surfaces. Moreover, the q profiles at the same time (shown in Fig. 7 (b) and Fig. 7 (c)) are flattened and almost equals unity inside the $q = 1$ surface, similar to the MHD result.
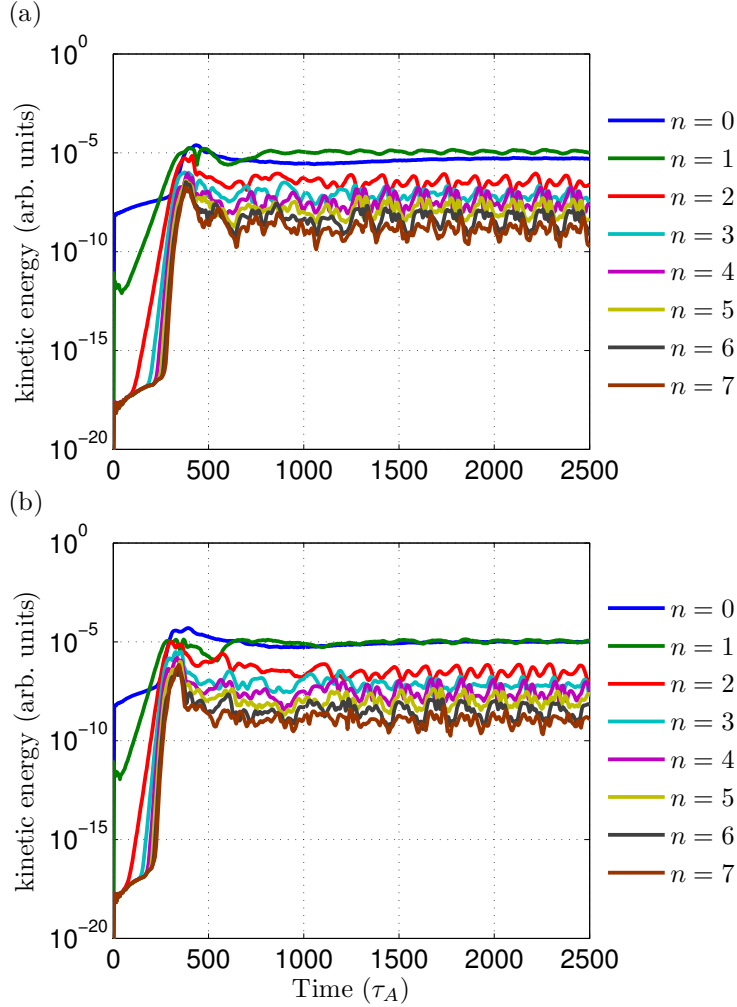
Figure 12: Kinetic energy of different toroidal modes versus time. (a) $\Delta\Psi = 0.39$ and $P_{beam,0}/P_{total,0} = 0.329$. (b) $\Delta\Psi = 0.25$ and $P_{beam,0}/P_{total,0} = 0.418$.

To investigate whether the saturation of the mode depends on the nonlinearity of energetic particles or MHD, The MHD response from the thermal plasmas is constrained to be linear by keeping only the $n = 1$ toroidal perturbation. As shown in Fig. 13, the $n = 1$ kinetic energy grows to a very large amplitude and does not saturate. This indicates that the saturation of the mode is due to MHD nonlinearity. Our results are different from typical fishbone results, in which the mode saturation is mainly due to nonlinear flattening of the energetic particle distribution function[29].
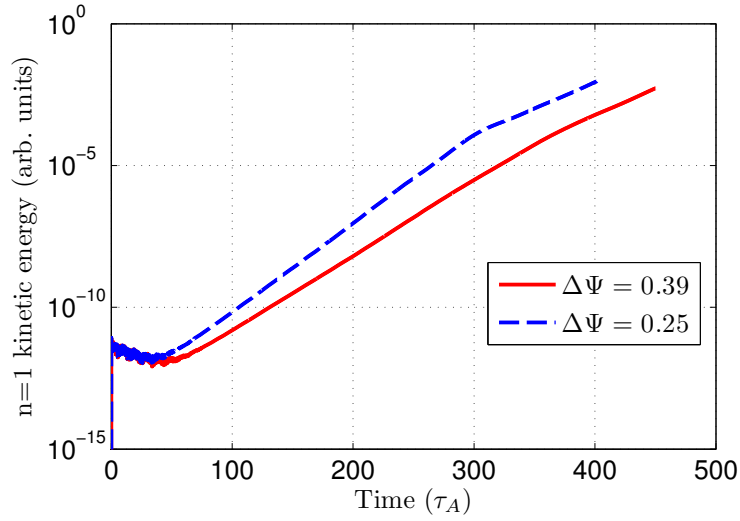
Figure 13: $n = 1$ kinetic energy versus time without MHD nonlinearity. The solid line (red) represents $\Delta\Psi = 0.39$ and $P_{beam,0}/P_{total,0} = 0.329$, while the dashed line (blue) represents $\Delta\Psi = 0.25$ and $P_{beam,0}/P_{total,0} = 0.418$.

Fig. 14 compares the $n = 1$ and $n = 0$ components of the kinetic energy with and without energetic beam ions. As shown in Fig. 14 (a), beam ions effects are destabilizing for the $n = 1$ mode during the linear phase and stabilizing during the nonlinear phase (i.e., reducing the nonlinear saturated level of the $n = 1$ mode). Furthermore, the saturation level of the $n = 0$ component is higher with beam ions, as shown in Fig. 14 (b). Fig. 14 also show that a narrower radial profile of beam ions leads to a stronger linear growth rate and a higher saturation level of the $n = 0$ component.
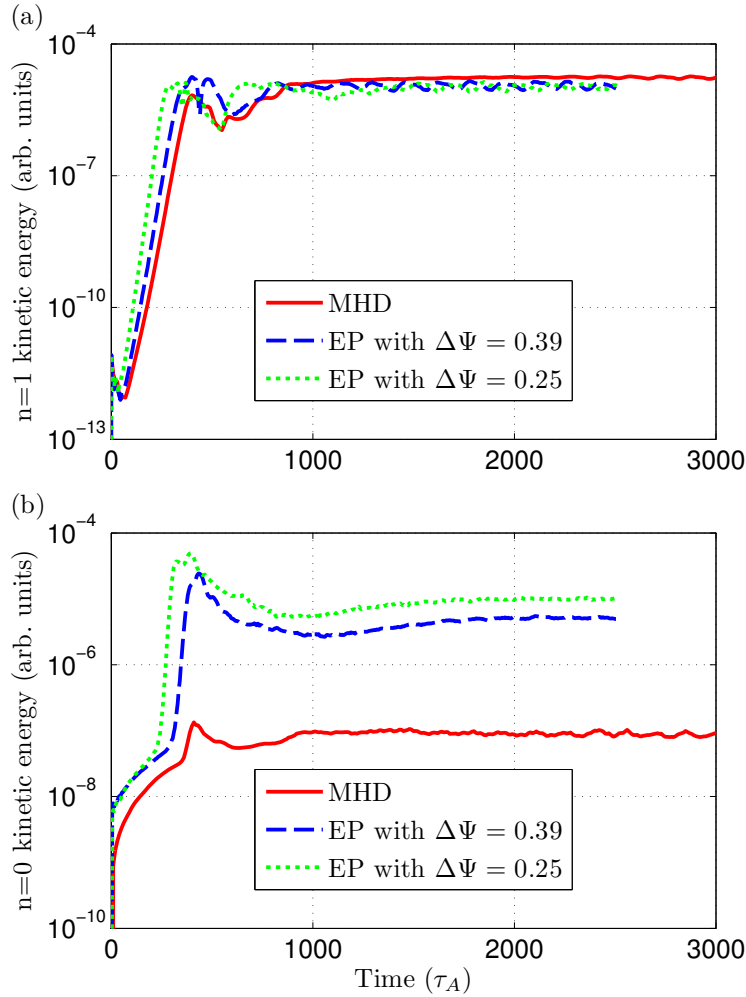
Figure 14: (a) The $n = 1$ kinetic energy versus time. (b) The $n = 0$ kinetic energy versus time.

We now discuss the dependence of mode frequency on beam ion pressure profile. Fig. 15 shows the evolution of the mode frequency for the two beam profiles. For the broader beam profile case, the mode frequency in the nonlinear phase is slightly lower than the initial linear frequency. However, for the narrower beam profile case, the mode frequency chirps down more significantly in the nonlinear phase.

To summarize the nonlinear results with beam ion kinetic effects, we find that the $n = 1$ mode with beam ion effects also leads to a quasi-steady state of saturated kink as in the MHD case in the last section. The main difference with the MHD results is that the 3D saturated kink mode now acquires a finite mode frequency due to the kinetic effects of beam ions. Also the mode frequency chirps down significantly during the nonlinear evolution for the case with a narrow beam profile. This result is consistent with the experiment observation that the so-called fishbone instability tends to appear with on-axis NBI injection where the beam profile is peaked near the axis.
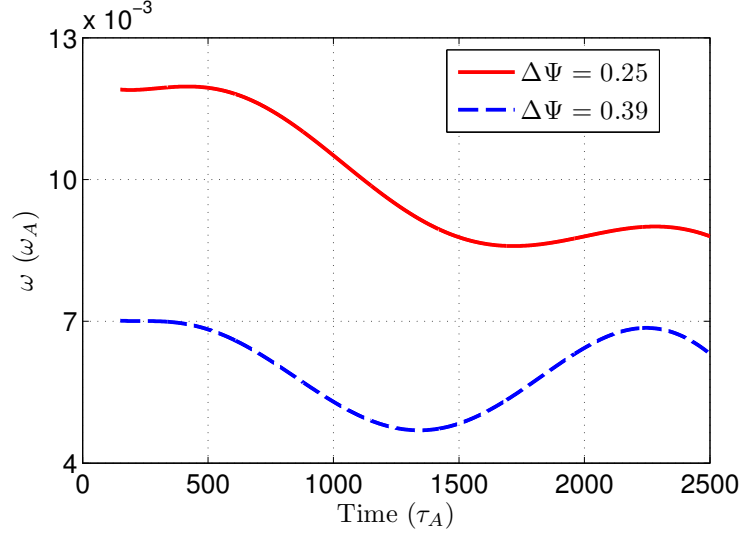
16

Figure 15: Nonlinear evolution of the mode frequency with two different beam radial profiles.

Finally we discuss the effects of the n=1 mode on the beam ion profile. Fig. 16 shows the redistribution of beam ions with $v = 0.705\, v_A$ due to the fishbone-like mode with $\Delta\Psi = 0.25$ and $P_{beam,0}/P_{total,0} = 0.418$. Note that the horizontal axis $P_\phi = e\Psi + Mv_\parallel RB_\phi/B$ is the toroidal angular momentum and can be regarded as a radial variable. First, after the initial sawtooth crash (at $t = 500\ \tau_A$), both of the co-passing and trapped particles are strongly redistributed inside the sawtooth region. Then, during the nonlinear saturation of the kink mode (from $t = 1500\ \tau_A$ to $t = 2500\ \tau_A$), the distribution of both co-passing and trapped particles becomes more flattened inside the $q = 1$ surface. According to previous work[36, 37, 38], the redistribution level of trapped particles decreases with increasing particle energy and a critical energy is obtained from the condition $\omega_{pr} = 2\pi/\tau_{cr}$, where ω_{pr} is the precessional frequency. The critical energy of trapped particles is given by

$$E_{crit} = 2\pi M\kappa_s r_s R_0 \omega_B/\tau_{cr}, \tag{6}$$

where M is the ion mass, κ is the ellipticity of the cross-section, ω_B is the cyclotron frequency, and the subscript 's' labels the values at the $q = 1$ flux surface. Assuming $\kappa_s \sim 1.3$, and $\tau_{cr} = 165\ \tau_A$ in our simulation, the calculated critical velocity of trapped particles is $v_{crit} = 0.803\ v_A$, which is a little larger than the velocity of beam ions shown in Fig. 16. As a result the trapped particles should be weakly redistributed, which seems to be contrary to our simulation results. However, when the frequency of the fishbone-like mode is considered, the condition $\omega_{pr} = 2\pi/\tau_{cr}$ is changed to $|\omega_{pr} - \omega| = 2\pi/\tau_{cr}$[34], where ω is the mode frequency. The frequency of the mode is estimated as $\omega = 0.012\ \omega_A$ during the initial sawtooth crash, and the calculated critical velocity of the trapped particles is modified to $v_{crit} = 0.921\ v_A$, which is consistent with the strong redistribution of the trapped particles with $v/v_A = 0.705$ in our simulation.
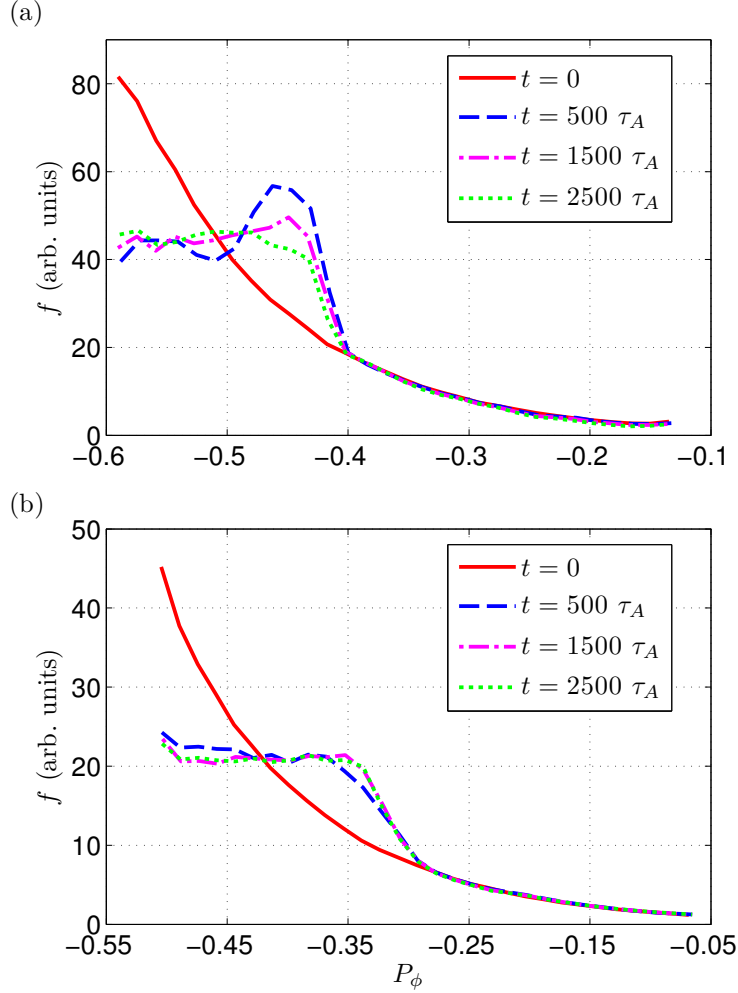
17

Figure 16: Beam ions redistribution induced by the fishbone-like mode with $\Delta\Psi = 0.25$ and $P_{beam,0}/P_{total,0} = 0.418$. (a) Co-passing particles with $\Lambda = 0.2$ and $v/v_A = 0.705$. (b) Trapped particles with $\Lambda = 1.0$ and $v/v_A = 0.705$.

5   DISCUSSION AND CONCLUSION

In this work we have performed a systematic study of linear and nonlinear dynamics of the $n = 1$ kink mode in DIII-D plasmas. Compared to previous work, realistic modeling of thermal plasma evolution using resistive MHD model and beam ion kinetic effects are considered in our simulation. Based on the parameters and profiles of a realistic DIII-D discharge plasmas, our results show that in MHD limit the $n = m = 1$ kink mode is ideally unstable, nonlinearly a quasi-steady state with the saturated kink mode has been found after the first sawtooth crash. Furthermore, with the kinetic effects of the beam ions, a fishbone-like mode is excited with mode frequency around a few kHz, and the mode frequency is larger with higher beam power and/or narrower radial profile of the beam pressure. Nonlinear simulations show that the fishbone-like mode could also transit to a saturated kink mode with a finite mode frequency

after the sawtooth crash. These results are consistent with the experimental observation of saturated kink mode between sawtooth crashes.

In our simulation, the resistivity values are not realistic and much larger than the experimental value because the experimentally relevant resistivity values are computationally prohibitive for the code. Furthermore the fast chirping dyanmics of the fishbone has not been reproduced. A proper modeling of the observed chirping fishbone requres much longer simulations with beam ion source and slow evolution of pressure profiles. This will be in future with necessary improvement in code efficiency.

In conclusion, nonlinear simulations of the n=1 kink mode have been carried out with or without beam ion kinetic effects using the kinetic-MHD code M3D-K for the parameters and profiles of a DIII-D sawteething discharge. The simulation results show that the n=1 kink/fishbone instability transits to a 3D quasi-steady state after an initial sawtooth crash. With beam ion kinetic effects, the saturated kink mode acquires a finite mode frequency on order of a few kHz. These results agree qualitatively with the experimental observation in the DIII-D plasmas.

ACKNOWLEDGEMENTS

References

[1] A. Weller, A. D. Cheetham, A. W. Edwards, R. D. Gill, A. Gondhalekar, R. S. Granetz, J. Snipes, and J. A. Wesson, Phys. Rev. Lett. 59, 2303 (1987).

[2] R. D. Gill, A. W. Edwards, D. Pasini, and A. Weller, Nucl. Fusion 32, 723 (1992).

[3] J. A. Wesson, Plasma Phys. Controlled Fusion 37, A337 (1995).

[4] A.-L. Pecquet, P. Cristofani, M. Mattioli, X. Garbet, L. Laurent, A. Geraud, C. Gil, E. Joffrin, and R. Sabot, Nucl. Fusion 37, 451 (1997).

[5] L. Delgado-Aparicio, L. Sugiyama, R. Granetz, D. A. Gates, J. E. Rice, M. L. Reinke, M. Bitter, E. Fredrickson, C. Gao, M. Greenwald, K. Hill, A. Hubbard, J. W. Hughes, E. Marmar, N. Pablant, Y. Podpaly, S. Scott, R. Wilson, S. Wolfe, and S. Wukitch, Phys. Rev. Lett. 110, 065006 (2013).

[6] H. Reimerdes, I. Furno, F. Hofmann, An Martynov, A. Pochelon, and O. Sauter, Plasma Phys. Control. Fusion 48, 1621 (2006).

[7] Y. Camenen, F. Hofmann, A. Pochelon, A. Scarabosio, S. Alberti, G. Arnoux, P. Blanchard, S. Coda, T. P. Goodman, M. A. Henderson, E. Nelson-Melby, L. Porte, and O. Sauter, Nucl. Fusion 47, 586 (2007).

[8] I. T. Chapman, M.-D. Hua, S. D. Pinches, R. J. Akers, A. R. Field, J. P. Graves, R. J. Hastie, C. A. Michael, and the MAST Team, Nucl. Fusion 50, 045007 (2010).

[9] J. E. Menard, R. E. Bell, E. D. Fredrickson, D. A. Gates, S. M. Kaye, B. P. LeBlanc, R. Maingi, S. S. Medley, W. Park, S. A. Sabbagh, A. Sontag, D. Stutman, K. Tritz, W. Zhu, and the NSTX Research Team, Nucl. Fusion 45, 539 (2005).

[10] J. A. Breslau, M. S. Chance, J. Chen, G. Y. Fu, S. Gerhardt, N. Gorelenkov, S. C. Jardin, and J. Manickam, Nucl. Fusion 51, 063027 (2011).

[11] S. P. Gerhardt, D. P. Brennan, R. Buttery, R. J. La Haye, S. Sabbagh, E. Strait, M. Bell, R. Bell, E. Fredrickson, D. Gates, B. LeBlanc, J. Menard, D. Stutman, K. Tritz, and H. Yuh, Nucl. Fusion 49, 032003 (2009).

[12] F. Wang, G. Y. Fu, J. A. Breslau, K. Tritz, and J. Y. Liu, Phys. Plasmas 20, 072506 (2013).

[13] F. Wang, G. Y. Fu, J. A. Breslau, and J. Y. Liu, Phys. Plasmas 20, 102506 (2013).

[14] R. Lorenzini, E. Martines, P. Piovesan, D. Terranova, P. Zanca, M. Zuin, A. Alfier, D. Bonfiglio, F. Bonomo, A. Canton, S. Cappello, L. Carraro, R. Cavazzana, D. F. Escande, A. Fassina, P. Franz, M. Gobbin, P. Innocente, L. Marrelli, R. Pasqualotto, M. E. Puiatti, M. Spolaore, M. Valisa, N. Vianello, P. Martin, and RFX-mod Team and Collaborators, Nat. Phys. 5, 570 (2009).

[15] W. A. Cooper, J. P. Graves, A. Pochelon, O. Sauter, and L. Villard, Phys. Rev. Lett. 105, 035003 (2010).

[16] W. A. Cooper, J. P. Graves, O. Sauter, I. T. Chapman, M. Gobbin, L. Marrelli, P. Martin, I. Predebon, and D. Terranova, Plasma Phys. Control. Fusion 53, 074008 (2011).

[17] W. A. Cooper, I. T. Chapman, O. Schmitz, A. D. Turnbull, B. J. Tobias, E. A. Lazarus, F. Turco, M. J. Lanctot, T. E. Evans, J. P. Graves, D. Brunetti, D. Pfefferlé, H. Reimerdes, O. Sauter, F. D. Halpern, T. M. Tran, S. Coda, B. P. Duval, B. Labit, A. Pochelon, M. R. Turnyanskiy, L. Lao, T. C. Luce, R. Buttery, J. R. Ferron, E. M. Hollmann, C. C. Petty, M. van Zeeland, M. E. Fenstermacher, J. M. Hanson, and H. Lütjens, Nucl. Fusion 53, 073021 (2013).

[18] J. E. Menard, R. E. Bell, D. A. Gates, S. M. Kaye, B. P. LeBlanc, F. M. Levinton, S. S. Medley, S. A. Sabbagh, D. Stutman, K. Tritz, and H. Yuh, Phys. Rev. Lett. 97, 095002 (2006).

[19] S. P. Gerhardt, D. A. Gates, S. M. Kaye, R. Maingi, J. E. Menard, S. A. Sabbagh, V. Soukhanovskii, M. G. Bell, R. E. Bell, J. M. Canik, E. Fredrickson, R. Kaita, E. Kolemen, H. Kugel, B. P. Le Blanc, D. Mastrovito, D. Mueller, and H. Yuh, Nuclear Fusion 51, 073031 (2011).

[20] Avinash, R. J. Hastie, J. B. Taylor, and S. C. Cowley, Phys. Rev. Lett. 59, 2647 (1987).

[21] M. N. Bussac and R. Pellat, Phys. Rev. Lett. 59, 2650 (1987).

[22] F. L. Waelbroeck, Phys. Fluids B 1, 499(1989).

[23] L. A. Charlton, R. J. Hastie, and T. C. Hender, Phys. Fluids B 1, 798 (1989).

[24] H. Lütjens and J. F. Luciani, J. Comput. Phys. 227, 6944 (2008).

[25] F. D. Halpern, D. Leblond, H. Lütjens, and J.-F. Luciani, Plasma Phys. Controlled Fusion 53, 015011 (2011).

[26] S. P. Hirshman and O. Betancourt, J. Comput. Phys. 96, 99 (1991).

[27] W. A. Cooper, S. P. Hirshman, P. Merkel, J. P. Graves, J. Kisslinger, H. F. G. Wobig, Y. Narushima, S. Okamura, K. Y. Watanabe, Comput. Phys. Commun. 180, 1524 (2009).

[28] W. Park, E. V. Belova, G. Y. Fu, X. Z. Tang, H. R. Strauss, and L. E. Sugiyama, Phys. Plasmas 6, 1796 (1999).

[29] G. Y. Fu, W. Park, H. R. Strauss, J. Breslau, J. Chen, S. Jardin, and L. E. Sugiyama, Phys. Plasmas 13, 052517 (2006).

[30] G. Y. Fu and W. Park, Phys. Rev. Lett. 74, 1594 (1995).

[31] J. A. Breslau, S. C. Jardin, and W. Park, Phys. Plasmas 14, 056105 (2007).

[32] J. Lang, G. Y. Fu, and Y. Chen, Phys. Plasmas 17, 042309 (2010).

[33] H. Cai and G. Y. Fu, Phys. Plasmas 19, 072506 (2012).

[34] W. Shen, G. Y. Fu, Z. M. Sheng, J. A. Breslau, and F. Wang, Phys. Plasmas 21, 092514 (2014).

[35] L. Chen, R. B. White, and M. N. Rosenbluth, Phys. Rev. Lett. 52, 1122 (1984).

[36] Y. I. Kolesnichenko, and Y. V. Yakovenko, Nucl. Fusion 36, 159 (1996).

[37] Y. I. Kolesnichenko, V. V. Lutsenko, Y. V. Yakovenko, and G. Kamelander, Phys. Plasmas 4, 2544 (1997).

[38] Y. I. Kolesnichenko, V. V. Lutsenko, R. B. White, and Y. V. Yakovenko, Nucl. Fusion 40, 1325 (2000).